JOURNAL OF MATERIALS SCIENCE **37** (2002) 4079–4091

Microstructural and analytical study of heavily faulted Frank-Kasper R-phase precipitates in the ferrite of a duplex stainless steel

A. REDJAÏMIA*
Laboratoire de Science et Génie des Surfaces, UMR-CNRS 7570. Ecole Européenne d'Ingénieurs en Génie des Matériaux, Ecole des Mines, Parc de Saurupt, F-54042 Nancy Cedex, France
E-mail: redjamia@mines.u-nancy.fr

J. P. MORNIROLI
Laboratoire de Métallurgie Physique et Génie des Matériaux, UMR-CNRS 8517, Université de Lille 1, Bâtiment C6, F-59655 Villeneuve d'Ascq Cedex, France

P. DONNADIEU
L. T. P. C. M. INPG-ENSEEG, UMR-CNRS-5614, 1130 rue de la piscine, BP75 Domaine universitaire F-38402 Saint Martin D'Hères Cedex, France

G. METAUER
Laboratoire de Science et Génie des Surfaces, UMR-CNRS 7570. Ecole Européenne d'Ingénieurs en Génie des Matériaux, Ecole des Mines, Parc de Saurupt, F-54042 Nancy Cedex, France

The ferritic matrix in the Fe-22Cr-5Ni-3Mo-0.03C ferritic-austenitic duplex stainless steel can undergo a variety of decomposition processes when aged in the temperature range 550–650°C. These processes are the precipitation of the γ_s austenitic bi-crystal, the α'-BCC ferrite, the τ-phase and the heavily faulted R-phase. The latter is a Frank-Kasper phase, which nucleates on the dislocations in the ferritic δ-matrix and adopts a lenticular shape. This study is basically focused on this intermetallic R-phase. The crystal structure and the chemical composition are respectively studied by electron microdiffraction and energy dispersive X-ray spectroscopy. The R-phase is oriented with respect to the surrounding ferritic matrix by developing a rational orientation relationship such that: $(0\,0\,0\,1)_R /\!/ (1\,1\,1)_\delta$ with $[1\,\bar{3}\,2]_\delta /\!/ [2\,\bar{1}\,\bar{1}\,0]_R$. This orientation relationship is here examined in term of lattice matching. Based on this orientation, the morphology and the variant number of this R-phase are understood in terms of the group theory. The defects, present in a large density in the R-phase, are identified as planar faults, which are grouped in two families parallel respectively to $\{1\,3\,9\}_\delta$ and $\{11\,13\,23\}_\delta$ lattice planes of the ferritic δ-matrix. Based on the obtained results, a structural proximity between the R-phase and a supercell derived from the ferritic matrix has been brought to light. It has been stated that Mo is an efficient R-phase forming element. The results provide valuable insights into the precipitation mechanism associated with the R-phase formation.

1. Introduction

Duplex stainless steels are being increasingly used as structural material in oil, chemical and power industries [1–4]. This is related to the fact that their duplex microstructure ($\delta + \gamma$) allows a beneficial mixture of austenitic (γ) and ferritic (δ) properties: on the one hand high strength with a desirable toughness [5, 6] and, on the other, good corrosion resistance, especially to chloride-induced stress corrosion cracking [7–9]. The Z3CND-22-05 with nominal composition (wt%) Fe-22Cr-5Ni-3Mo-0.03C is a member of this family. This grade is now largely used as a standard material in offshore conditions [10]. The heat treatment of this duplex stainless steel leads to a series of metallurgical transformations, which take place in the ferrite or at its grain boundaries, apart from the martensite, which forms in the austenite grains [11, 12]. In a detailed study [13], efforts were made to characterize the different products of the δ-ferritic matrix decomposition in the temperature range 400–1050°C. The characterization

*Author to whom all correspondence should be addressed.

of the phase precipitation was best undertaken by an isothermal heat treatment from the fully δ-ferrite microstructure retained by water quenching to ambient temperature from the solutionizing single domain. This isothermal treatment induces the decomposition of the supersaturated δ-ferrite. The various identified phases include $M_{23}C_6$ and M_7C_3 type carbides [11], austenite (γ) with different shapes [11, 12, 14], the α'-BCC ferrite [11, 15] being responsible for the well-known embrittlement at 475°C in Fe-Cr system [16], the intermetallic G-phase [17], the novel τ-phase described elsewhere [18] and the undesirable secondary precipitates. The latter being the intermetallic phases: sigma (σ), chi (χ) and R [19].

The intermetallic R-phase, the characterization of which is reported in this paper belongs to the tetrahedrally close-packed (TCP) phases. It has been shown by Frank and Kasper [20] that the TCP phases have very particular long-range properties deriving from the local tetrahedral requirement. The crystallographic structure of the R-phase has been determined by Komura *et al.* [21] using single crystal X-ray analysis and by Shoemarker *et al.* [22] using powder neutron diffraction. According to the former authors [21], the atomic decoration of the rhombohedral unit cell of the R-phase can be described as a sequence of five coordination shells or five polyhedra along the 3-fold axis: the 000 node is occupied by a Coordination Number 16 coordination (CN16) shell followed by three CN12 shells and finally the sequence is completed by another CN16 shell. In fact, this decoration gives rise to an efficient tetrahedral packing of the atoms. The chain of polyhedra, the sequence of which is: CN16-CN12-CN12-CN12-CN16, includes all the 53 atoms in the rhombohedral unit cell, 27 of them having a 12-fold coordination shell [21]. In fact, the structure of the R-phase is closely related to those of other transition-group phases such as σ, P, χ and μ phases [20].

Several investigations [23–28] have been reported and have dealt with the R-phase precipitation during the isothermal heat treatment in steels. However, a complete crystallographic study of the intermetallic R-phase in any kind of stainless steels was not carried out. A detailed characterization is of extreme significance because it is expected to provide valuable insights into the precipitation mechanism associated with the R-phase formation.

Thus, the objective of this investigation is basically to characterize the intermetallic R-phase precipitated within the ferritic δ-matrix of a duplex stainless steel as a consequence of isothermal heat treatment. The crystal structure of such a R-phase has been achieved by X-ray [21] and neutron diffraction [22] but never by electron diffraction. We intend, in this study, to determine, in greater detail, by TEM and electron diffraction the crystal structure and microstructure of the R-phase, and thus to test the results established by the two previous studies [21, 22]. The derived information will be used as a basis for studying the structural similitudes between the R-phase and the ferritic δ-matrix where it takes place.

TABLE I Chemical composition (wt%) obtained from EDS on a specimen before ageing and after ageing at 650°C for 336 hours

	Fe	Mo	Cr	Mn	Ni	Si
The R-phase	42.15	29.5	19.30	2.85	5.11	0.75
The δ-matrix	68.21	1.63	21.20	2.84	5.24	0.70
δ Quenched	68.75	2.55	2.55	1.63	5.01	0.46

2. Material and experimental procedure

The as-received duplex austenitic-ferritic ($\delta + \gamma$) stainless steel, the chemical composition of which is given in Table I, was solution treated at 1375°C for 20 min to achieve homogeneity and subsequently water-quenched to retain a supersaturated and fully ferritic (δ) microstructure. Specimens were then treated in the temperature range 550–650°C for various times up to 336 hours, followed by water-cooling. All the treatments were carried out in electric muffle furnaces under vacuum to minimize oxidation.

Thin foils were prepared following conventional transmission electron microscopy (TEM) sample preparation methods. The metallographic samples were first ground to about 20 μm thickness. Then, they were electropolished in a Struers Tenupol twin jet unit operating at 40 V potential and using a solution of 5% perchloric acid in 95% II-butoxyethanol. They were investigated in two transmission electron microscopes: a Philips CM12 microscope operated at 120 kV and a Jeol 200 CX microscope operated at 200 kV. A double tilt specimen holder was used. The diffraction patterns were obtained in the convergent beam electron diffraction (CBED) mode with a nearly parallel beam focused on a very small area of the thin foil. High-resolution electron microscopy (HREM) was performed on a Philips EM 430 ST electron microscope operated at 300 kV. The optimum point-to-point resolution was better than 0.2 nm. This instrument was equipped with a Tracor-Northern energy-dispersive X-ray spectroscopy (EDS) analysis system. The EDS spectrometer is interfaced with a minicomputer to log the spectra and to conduct qualitative or quantitative analyses. Quantitative analysis of EDS spectra without standards was performed assuming the thin film approximation of no absorption. The Cliff-Lorimer expression for concentration ratios was used, relying on k factor values calculated for K spectral lines.

An X-ray diffractometer, equipped with a Co K_α source, was used to determine with accuracy the lattice parameter of the body centred cubic (BCC) ferritic matrix.

3. Experimental results

Starting from the supersaturated and fully ferritic matrix, the isothermal heat treatment in the temperature range between 550 and 650°C leads, after exposures up to 336 hours, to different metallurgical transformations:

- The precipitation of γ_s austenitic bi-crystals displaying twin related orientation in the ferritic

matrix [14]. Contrary to the austenite precipitating at high temperature (750–970°C), the formation of this austenite operates through the following steps: (i) enrichment of {110}-planes in ferrite with γ-forming elements by diffusion, (ii) double shear to change from BCC (δ) to FCC (γ) lattice, (iii) twinning of the FCC (γ) structure to reduce local strains and deformation of γ bi-crystals, (iv) growth of the twinned γ bi-crystals towards the ferritic matrix by volume diffusion.

- The precipitation of the τ-phase, a novel intermetallic compound [18], exhibiting a needle like morphology and belonging to the *Fmmm* space group with the following lattice parameters: $a = 0.4054$ nm, $b = 0.3436$ nm and $c = 0.2867$ nm. The τ-phase precipitation occurs by a diffusional process.
- The α'-BCC ferrite [15] which is known to be responsible for the embrittlement at 475°C in Fe-Cr system [16].
- The precipitation of the Frank-Kasper R-phase the crystal structure of which is trigonal and described by a rhomobohedral unit cell with $a = 0.901$ nm and $\alpha = 74°30$ containing 53 atoms. This phase can also be described using a triple obverse or reverse hexagonal unit cell. In this paper, the triple obverse hexagonal unit cell is used to describe the R-phase with $a = 1.090$ nm and $c = 1.934$ nm. The latter contains three times as many atoms as the rhombohedral one, i.e., $3 \times 53 = 159$ atoms. These crystallographic data are in agreement with those of the R-phase which was first reported in 1951 by Rideout *et al.* [29] in Cr-Mo-Co ternary alloy and whose $R\bar{3}$ space group was determined by Komura *et al.* [21] using X-ray diffraction and later by Shoemaker *et al.* using neutron diffraction [22].

It is well known that the precipitation of the intermetallic compounds causes the embrittlement of the alloys. Nilsson *et al.* [30] established that this intermetallic R-phase is a molybdenum rich compound which contributes to embrittlement and pitting corrosion in duplex stainless steel aged isothermally in the range 550–700°C. The brittleness and pitting corrosion are connected with the nucleation characteristics, microstructural distribution, and morphology as well as with their crystallographic orientation relationships, and the lattice misfit.

Thus, this investigation is intended to characterize, by TEM and electron diffraction, the crystallographic structure of the intermetallic R-phase precipitated within the ferritic matrix of a duplex stainless steel as a consequence of isothermal heat treatment. Such information is then used as a basis for studying the structural similitudes between the R-phase and its parent phase, the ferritic matrix.

3.1. Characterization of the R-phase

The isothermal heat treatment, in addition to γ_s austenitic bi-crystal [14], α'-BCC ferrite [15] and τ-phase [18], creates very fine and heavily faulted particles of the R-phase throughout the δ-matrix (Fig. 1). In the early precipitation stage, some particles are observed at the δ/δ grain boundaries and at the δ-twin interfaces (Fig. 2). With increasing ageing times, TEM observations show that the R-phase particles adopt a lenticular shape (Fig. 3) and gradually coarsen to approach a blocky shape. The precipitation reactions displayed C-curve kinetics with the nose of all the curves located around 600°C [13]. The incubation time at 600°C is estimated around 85 hours; it corresponds to the formation of R-phase particles detectable by TEM observations. After longer ageing times, light and TEM microscopies point out that the equilibrium R-phase is the dominant constituent. It exhibits coarsening particles in the vicinity of the austenite at the higher temperatures of the C-curve domain. Systematic

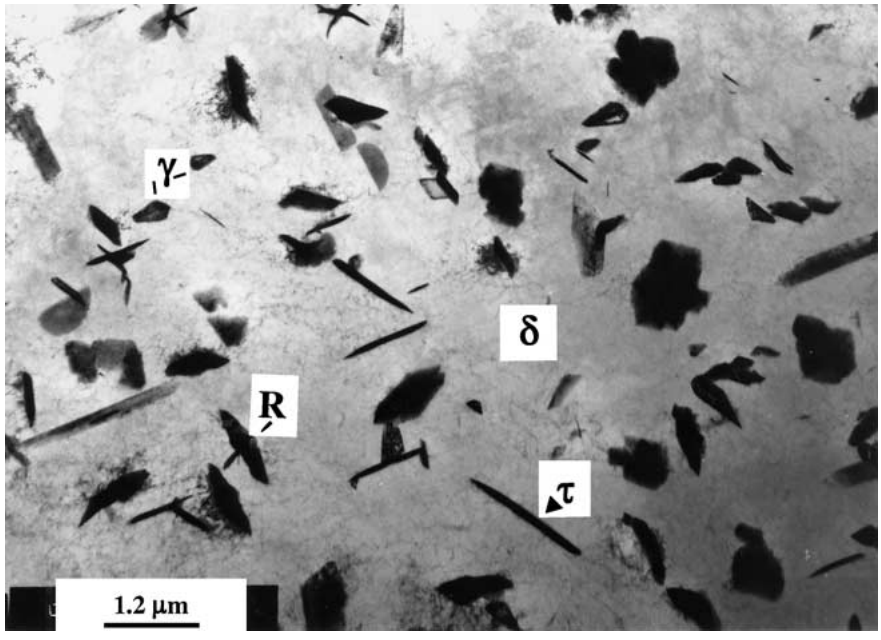

Figure 1 Bright field TEM image showing that an isothermal heat treatment leads to the formation of the γ_s austenitic bi-crystals, the τ-phase and particles of the R-phase throughout the δ-matrix.

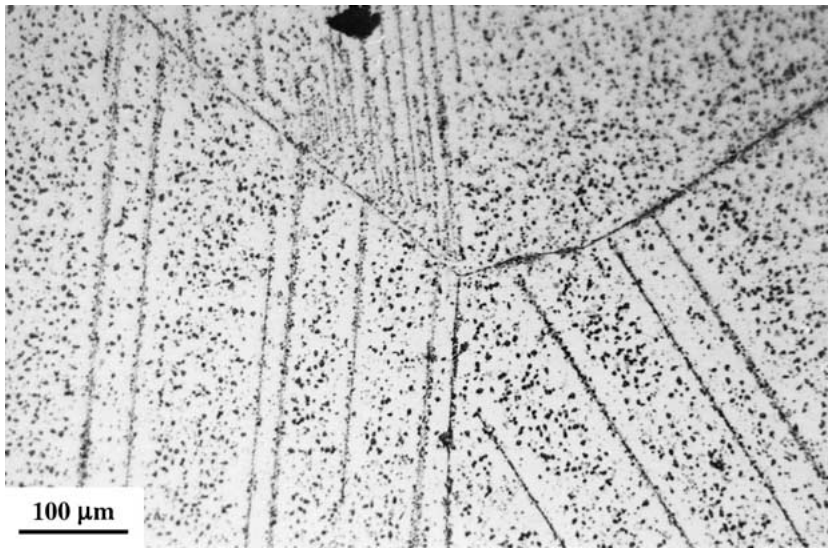

Figure 2 Light micrograph showing very fine precipitates of the R-phase throughout the δ-matrix, at the δ/δ grain boundaries and at the δ-twin interfaces.

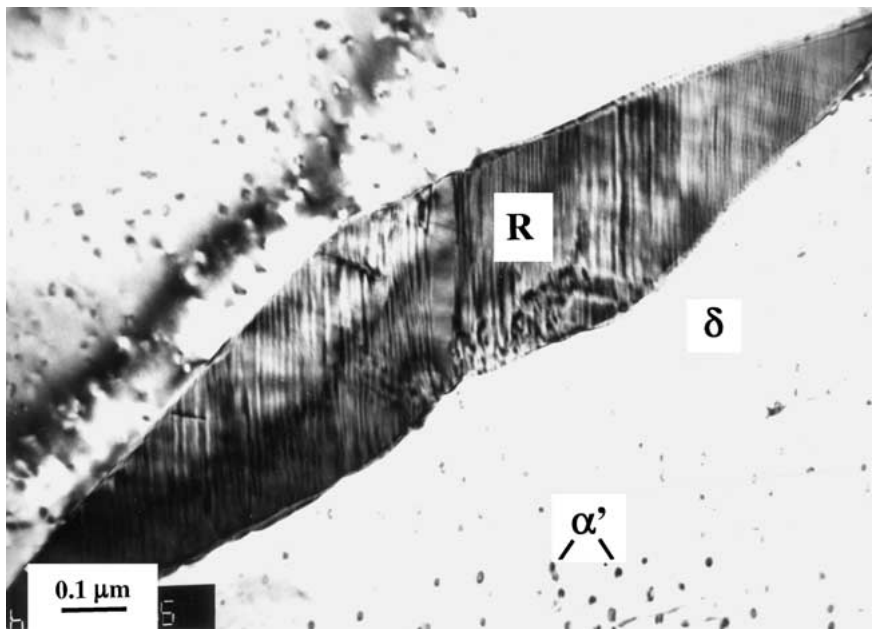

Figure 3 Bright field TEM image showing a lenticular R-phase particle embedded in the δ-ferritic matrix. The lenticular R-phase is extended along the $\langle 1\,1\,1\rangle$ directions of the matrix. The fine lines visible inside of the R-phase particle are indicative of extremely thin planar faults. Note the presence of α'-BCC ferrite particles around the R-phase particle.

tilting to two-beam conditions in different orientations reveals that R-phase particles present a rough contrast and nucleate on dislocations [13]. A recent study [31] has shown that cold work prior to ageing heat treatment significantly increases the number of R-phase particles. This experimental evidence strongly supports the fact that R-phase particles effectively nucleate on ferrite dislocations as reported by Haudin and Montheillet [27]. TEM observations and electron diffraction investigations show that the lenticular R-phase precipitates are extended along $\langle 111\rangle_\delta$ directions in the ferritic matrix (Fig. 3). This extending, which corresponds to the growth direction, was determined by trace analysis involving several orientations of δ-matrix grains.

3.2. Electron diffraction characterization

The structure of the R-phase has been only achieved by X-ray [21] and neutron diffraction [22] but never by electron diffraction. We intend, in this section, to determine, in greater detail, the crystal structure by electron diffraction, confirming thus the results obtained by the earlier authors.

Two-dimensional (2D) and especially three-dimensional (3D) symmetry information, required to determine completely the crystal structure of the R-phase precipitated as very small particles, is unfortunately not present in convergent beam electron diffraction (CBED) patterns. Morniroli and Steeds [32] have shown that crystal structure characterization, in such a case, may be achieved through microdiffraction

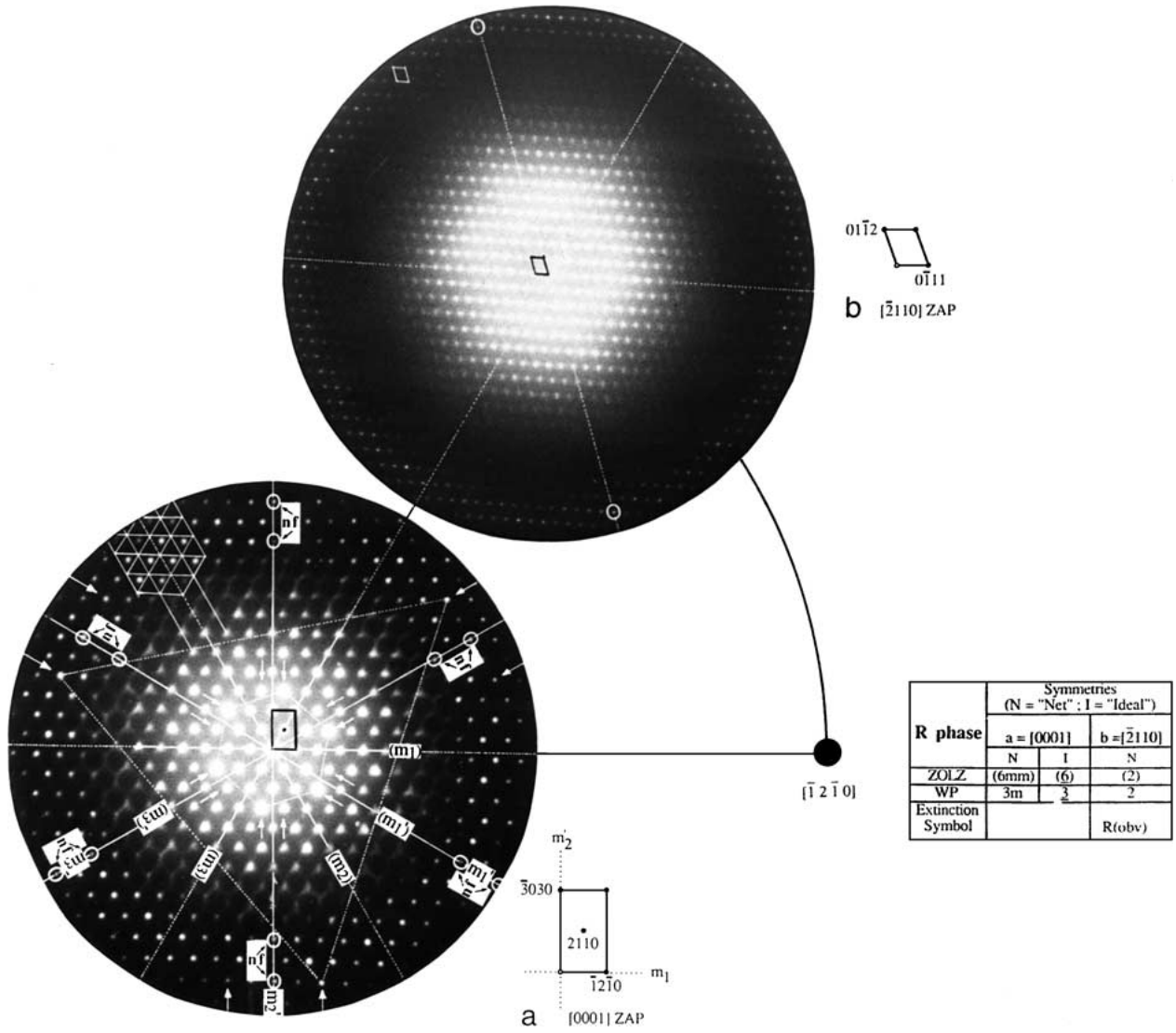

R phase	Symmetries (N = "Net" ; I = "Ideal")		
	a = [0001]		b = [$\bar{2}$110]
	N	I	N
ZOLZ	(6mm)	$(\underline{6})$	(2)
WP	3m	$\underline{3}$	2
Extinction Symbol			R(obv)

Figure 4 Whole patterns (ZOLZ + FOLZ symmetry information) for the trigonal R-phase: (a) [0001] zone axis microdiffraction pattern, showing {(6*mm*), 3*m*} "net" and {($\underline{6}$), $\underline{3}$} "ideal" symmetries. (b) [$\bar{2}$110] zone axis microdiffraction pattern, showing (2) and 2 "net" symmetries. It reveals no periodicity difference between the ZOLZ and the FOLZ. The deduced extinction symbol is *R*(*obv*)−−.

patterns obtained by focusing a nearly parallel electron beam onto a very small specimen area. The zone axis microdiffraction patterns thus obtained are composed of small diameter discs grouped into ZOLZ and HOLZ (zero and high order Laue zones, respectively). From the information of these whole patterns (WP), it is possible to determine the following crystallographic features.

- The "net" and "ideal" symmetries that are concerned, respectively, with the position and both the position and the intensity of the reflections on the microdiffraction pattern. These symmetries are in connection with the crystal system and the point group, respectively.
- The shift between the ZOLZ and the FOLZ (first order Laue zone) reflection nets. This shift is related to Bravais lattices.
- The periodicity difference between the ZOLZ and the FOLZ reflection nets. This difference is in connection with the presence of glide planes.

In such a way, the crystallographic features of the R-phase were determined from the recorded microdiffraction patterns by a systematic method given in detail elsewhere [32]. Among the investigated zone axis patterns (ZAPs) of the R-phase, it appears that the highest "net" symmetry has a (6*mm*) symmetry for the ZOLZ and a 3*m* symmetry for the whole pattern (WP) (Fig. 4a). For this pattern, the reflection of the FOLZ are situated in the centroids of the equilateral triangles formed with the net of the ZOLZ reflections. In addition, no pattern with (4*mm*), 4*mm* "net" symmetry has been observed. These features indicate, in accordance with Table 7 and Fig. 5b in Ref. [32], that the crystal system is trigonal and the lattice is rhombohedral. From Table 2 of Ref. [32] it is also deduced that the experimental pattern of (Fig. 4a) corresponds to the [0 0 0 1] zone axis.

For the trigonal system with rhombohedral lattice, the identification of the glide planes requires examination of the $\langle 1\,1\,\bar{2}\,0\rangle$ ZAPs (see Table 5 in Ref. [32]). Analysis of the [$\bar{2}$ 1 1 0] ZAP, which exhibits (2), 2 "net" symmetries (Fig. 4b), reveals no periodicity difference between the ZOLZ and the FOLZ reflection nets. In fact, since the lattice is described by means of a triple hexagonal obverse cell, the Laue zone which appears on the diffraction pattern is not the first-order Laue zone

TABLE II Space groups and point groups corresponding to the extinction symbol $R(obv)--$

Extinction symbol	Space groups	Point groups
	$R3$	3
	$R\bar{3}$	$\bar{3}$
$R(obv)--$	$R32$	32
	$R3m$	$3m$
	$R\bar{3}m$	$\bar{3}m$

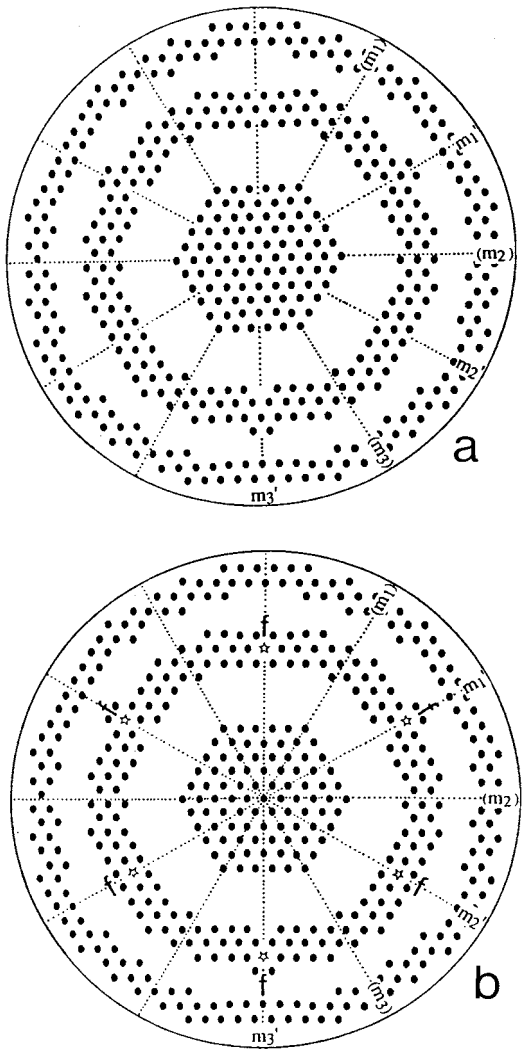

Figure	a	b
ZAP	[0001]	
Extinction Symbol	$R(obv)--$	$R(obv)-c$

Figure 5 (a, b) Theoretical [0001] ZAPs related to the $R(obv)--$ and $R(obv)-c$ extinction symbols. Forbidden reflection, labelled f, are situated on the m'_1, m'_2 and m'_3 mirrors in the FOLZ for the $R(obv)-c$ extinction symbol.

but the third one (TOLZ). From comparison with Fig. 9 in Ref. [32], it is concluded that the extinction symbol is $R(obv)--$. As indicated by Table 3.2 of the International Tables for Crystallography [35], this extinction symbol is in agreement with 5 space groups belonging to 5 point groups (Table II).

To make the distinction between these five possible space groups, the point group must be identified from observation of the "ideal" symmetries. The ZOLZ and whole pattern "ideal" symmetries for [0 0 0 1] ZAP are respectively $(\underline{6})$ and $\underline{3}$ as illustrated in (Fig. 4a) (see particularly some examples of difference of intensity between several couples of arrowed reflections which prove the absence of "ideal" mirrors if intensity is taken into account). According to Table 8 in Ref. [32], the point group is $\bar{3}$. Therefore the space group for the R-phase is $R\bar{3}$.

The extinction symbol $R(obv)--$ can also be identified and distinguished from the other possible extinction symbol $R(obv)–c$, by observing the [0001] ZAP. On this ZAP half of the reflections of the FOLZ situated on the three mirrors m'_1, m'_2 and m'_3 are forbidden reflections in the case of the extinction symbol $R(obv)–c$ (Fig. 5a) while no forbidden reflections exist in the case of $R(obv)--$ (Fig. 5b). We verified on well-oriented diffraction patterns that all the ZOLZ reflections present on these three mirrors (reflections noted nf in (Fig. 4) are not forbidden reflections. Their intensity does not decrease or vanish when the m' mirrors are accurately set parallel to the electron beam. This fact confirms that the extinction symbol is $R(obv)--$.

This characterization leads to the unambiguous conclusion that the space group for the R-phase is $R\bar{3}$. These electron diffraction results are in agreement with those established by Komura *et al.* [21] using X-ray diffraction and by Shoemaker *et al.* [22] using neutron diffraction.

The δ-matrix lattice parameter, $a_\delta = 0.2867$ nm, characterised by X-ray diffraction, is used to calibrate the electron diffraction patterns and to deduce the lattice parameters of the R-phase, namely, $a_R = b_R = 1.07$ nm and $c_R = 1.987$ nm.

All the theoretical electron diffraction patterns were performed using the Electron diffraction software [32].

3.3. Orientation relationship

It is experimentally obvious that R-phase precipitates have a definite orientation relationship with respect to the δ-matrix (Fig. 6).

The frequent overlapping of spots arising from the δ-matrix and from the R-phase indicates that many lattice planes from the two phases are parallel and have identical interplanar spacings. To find them experimentally and easily, the specimen is tilted until intersections of Bragg extinction contours from the δ-matrix are superimposed on R-phase particles.

The orientation relationship is deduced from diffraction patterns recorded on different particles and for a variety of incident beam directions (Fig. 6). The derived orientation relationship expressed by exact parallelism between the corresponding planes and exact parallelism between directions lying in these planes, can be quoted by the following:

$$(0\,0\,0\,1)_R /\!/ (1\,1\,1)_\delta$$

$$[2\,\bar{1}\,\bar{1}\,0]_R \equiv [1\,0\,0]_R /\!/ [1\,2\,\bar{3}]_\delta$$

$$\lfloor \bar{1}\,2\,\bar{1}\,0 \rfloor_R \equiv [0\,1\,0]_R /\!/ [\bar{3}\,1\,2]_\delta$$

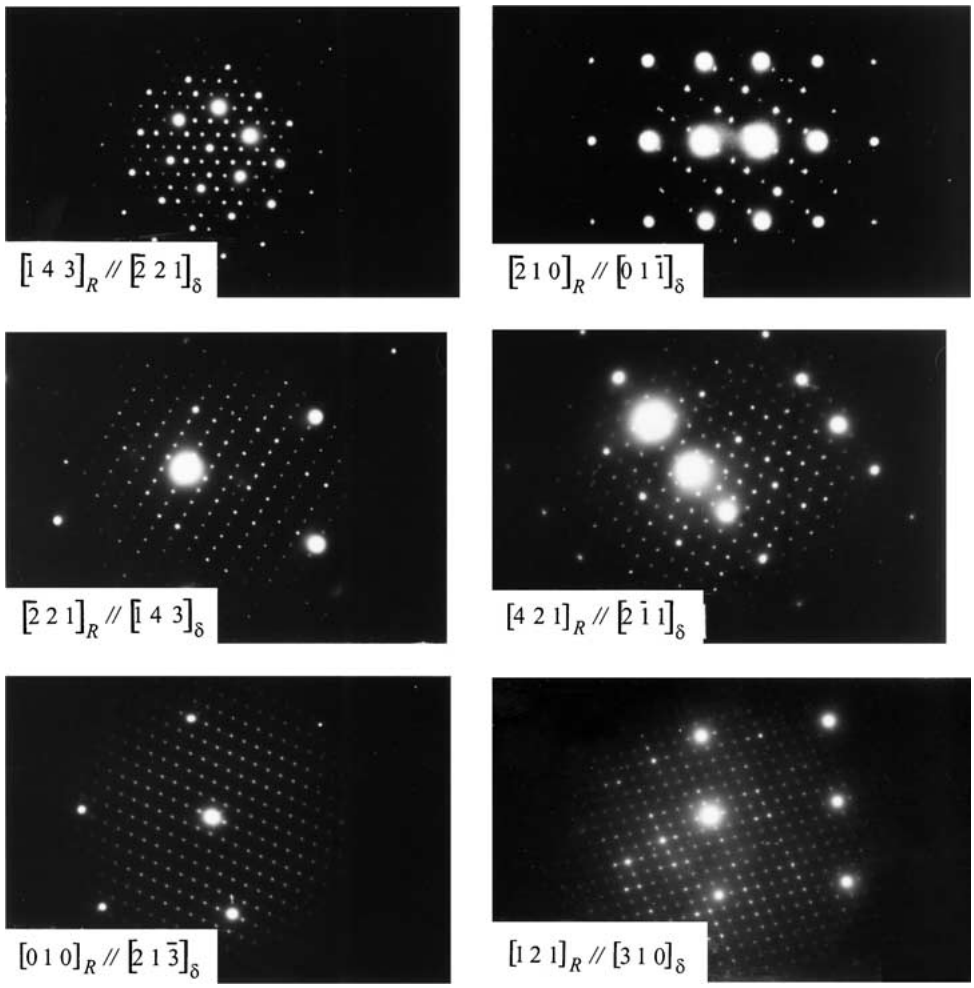

Figure 6 Series of composite electron diffraction patterns recorded along different zone axes common to R-phase particles and the surrounding δ-ferritic matrix. Many crystallographic planes which are parallel in the R-phase and in the δ-ferritic matrix have identical interplanar spacings.

For the R-phase, planes and directions are expressed with hexagonal axes. However for convenience, directions are given with three and four-digit indices (Weber nomenclature) and plane with four-digit indices (Miller-Bravais indices). This experimental orientation relationship is similar to that reported by Dyson *et al.* working with a 12% Cr-Co-Mo steel samples [24]. Contrary to our results, the latter authors indicated that exact parallelism between planes and directions is seldom seen in the diffraction patterns. However, Nilsson *et al.* [30] found the relation $(0\,0\,0\,1)_R /\!/ (\bar{1}\,1\,\bar{1})_\delta$ with $[1\,\bar{1}\,0\,0]_R /\!/ [1\,0\,\bar{1}]_\delta$, whereas Kobayashi *et al.* [28] found that the R-phase is related to the ferritic matrix by $(0\,0\,0\,1)_R /\!/ (\bar{1}\,\bar{1}\,1)_\delta$ with $[1\,1\,\bar{2}\,0]_R /\!/ [2\,\bar{3}\,\bar{1}]_\delta$. The deviation between these two orientations is estimated to be 10° around the 3-fold axis, $[0\,0\,0\,1]_R /\!/ [\bar{1}\,\bar{1}\,1]_\delta$. This deviation is attributed by the latter authors to experimental errors due to the intersection between Ewald sphere and significantly large reciprocal lattice.

In order to understand the discrepancy in the orientation relationship, attention has been focused on the experimental electron diffraction patterns (Fig. 6). Detailed analysis of the latter indicates that the R-phase is related to the surrounding δ-matrix by a parallelism between the following directions:

$$[\bar{3}\,1\,2]_\delta /\!/ [0\,1\,0]_R \equiv [\bar{1}\,2\,\bar{1}\,0]_R$$
$$[1\,2\,\bar{3}]_\delta /\!/ [1\,0\,0]_R \equiv [2\,\bar{1}\,\bar{1}\,0]_R$$
$$[1\,1\,1]_\delta /\!/ [0\,0\,1]_R \equiv [0\,0\,0\,1]_R$$

For the R-phase, the directions are expressed with hexagonal axes, using three-digit and four-digit indices to make the symmetry relationship between the directions immediately obvious. Let us note, that the 3-fold axis of the rhombohedral unit cell of the R-phase is set parallel to one of the four 3-fold axes of the cubic ferritic matrix.

In order to compare the present results with data reported in the literature, the corresponding orientations had to be transformed into the coordinate system adopted in the present study. This can readily be seen in Fig. 10b from which it turned out that the Kobayashi *et al.* orientation $(1\,1\,1)_\delta /\!/ (0\,0\,0\,1)_R$ with $[3\,\bar{2}\,\bar{1}]_\delta /\!/ [1\,1\,\bar{2}\,0]_R$ is the same as the one established in this study, whereas the orientation $(1\,1\,1)_\delta /\!/ (0\,0\,0\,1)_R$ with $[2\,1\,0]_\delta /\!/ [1\,0\,\bar{1}\,0]_R$ obtained by Nilsson *et al.* deviates from it by exactly 10.89°. In fact, as indicated in Fig. 10b, $[3\,2\,0]_R \equiv [4\,1\,\bar{5}\,0]_R$ is parallel to $[1\,\bar{1}\,0]_\delta$ and $[2\,1\,0]_R \equiv [1\,0\,\bar{1}\,0]_R$ is parallel to $[4\,\bar{5}\,1]_\delta$. However, it is noted that the electron diffraction patterns shown in

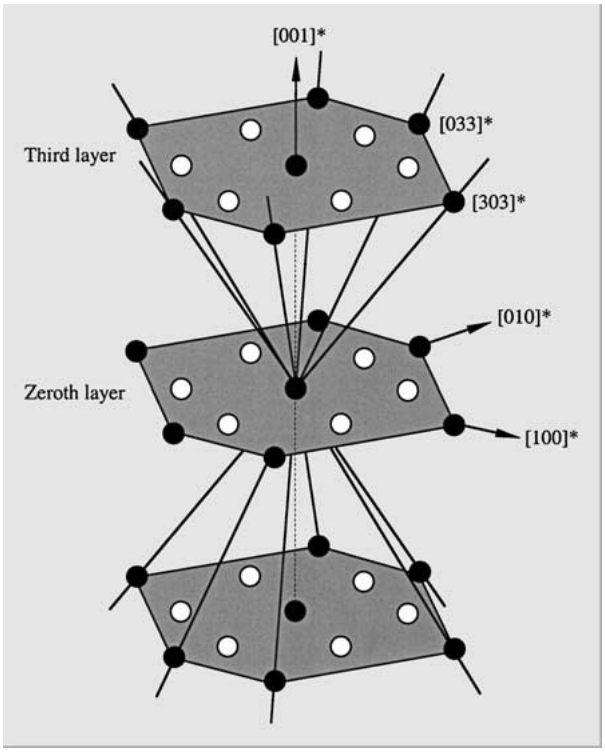

Figure 7 Schematic representation of the reciprocal lattice showing the diffuse streaks due to the planar defects, which are responsible for the honeycomb network observed on the diffraction pattern recorded along $[1\,1\,1]_\delta /\!/ [0\,0\,0\,1]_R$.

the paper of Nilsson *et al.* appear to be identical to that reported in this work. This might suggest that the orientation derived by Nilsson *et al.* has to be re-evaluated. The orientation relationship determined in this study confirms the result established first by Dyson *et al.* and later by Kobayashi *et al.* This orientation relationship is energetically favourable because there is a great variety of well matching δ-matrix and R-phase planes. Moreover, this orientation is characterised by a fairly low misfit $\Delta(\Delta = \frac{P^R_{[uvw]} - P^\delta_{[uvw]}}{P^\delta_{[uvw]}})$, between parallel directions. This low linear dilatation explains the favoured passage from the δ-matrix to the R-phase. This transition will be tackled in the following section.

3.4. Transition from a ferritic supercell to the R-phase

By considering the parallelism between directions given in the Section 3.3, it is convenient to use the matrix form to express the orientation between the R-phase and the δ-matrix. This will be particularly helpful in order to transform any plane or direction from the R-phase to the cubic system of the ferrite. The relationship respectively between the planes (hkl) and the directions $[uvw]$ in the two lattices can be written as:

$$(hkl)_R /\!/ M(hkl)_\delta \qquad (hkl)_\delta /\!/ M^{-1}(hkl)_R$$
$$[uvw]_\delta /\!/ M^t[uvw]_R \qquad [uvw]_R /\!/ M^{t^{-1}}[uvw]_\delta$$

If we take into account the parallelism between the directions mentioned previously and the lattice parameters a_δ, $a_R = b_R$ and c_R, we obtain the following matrix M:

$$(M) = \begin{pmatrix} 1 & -3 & 2 \\ 2 & 1 & -3 \\ 4 & 4 & 4 \end{pmatrix}$$

The determinant of this matrix, the value of which is equal to 84, indicates that the number of atoms in the R-phase is 84 times as much as in the δ-ferritic matrix, i.e., $84 \times 2 = 168$ atoms (the BCC ferritic matrix has 2 atoms per unit cell). This number is very close to the atomic number (159) of the R-phase as reported in the literature [20, 21].

As indicated by the matrix M, the lattice parameters a_R, b_R and c_R, expressed in the hexagonal axis system, are respectively set parallel to $\lfloor 1\,\bar{3}\,2 \rfloor_\delta$, $[2\,1\,\bar{3}]_\delta$ and $[1\,1\,1]_\delta$ with respect to the cubic system. The magnitude of the unit vector c_R is 4 times the length of the vector $a_\delta[1\,1\,1]_\delta$. The lattice parameter of the δ-matrix, calculated from X-ray diffraction patterns, was found to be $a_\delta = 0.2867$ nm [13]. Hence, the deduced R-phase lattice parameters, expressed in the hexagonal system are: $a_R = b_R = 1.07$ nm and $c_R = 1.987$ nm. One can notice that these values are very close to that given in the literature for the R-phase [20, 21].

In seeking to understand why the orientation relationship is favoured, reference may be made to a previous study conducted by Dyson *et al.* [24]. Indeed, the fact that parallelism is observed between many planes and many directions indicates clearly that the R-phase can be considered as a supercell of the ferritic matrix, the lattice parameters of which are $a_R = a_\delta\,[1\,\bar{3}\,2]_\delta$, $b_R = a_\delta\,[2\,1\,\bar{3}]_\delta$ and $c_R = 4a_\delta\,[1\,1\,1]_\delta$ and the angle between the two former basic vectors being 120° (Fig. 10b). This ferritic supercell can be considered as a stacking of 24 equally spaced atomic layers parallel to $(1\,1\,1)_\delta$ planes. These planes are parallel to the $(0\,0\,0\,1)_R$, basal planes of the R-phase. Each layer contains 7 atoms as illustrated in (Fig. 10b). In this figure, a schematic representation of the atoms projection onto $(1\,1\,1)_\delta$ planes of the ferritic matrix is drawn. The dark grey lozenge delimited by the bold solid lines corresponds to the unit cell of the ferritic supercell. Thus the number of the atoms in this unit supercell is quoted to be $24 \times 7 = 168$ atoms. The distance between two adjacent stacked atomic layers is $\frac{1}{6}a_\delta\,[1\,1\,1] = 0.082$ nm, i.e., ($c_R = 24 \times 0.082$ nm $= 0.1986$ nm). This assumption leads to an atomic excess of 5% and departures from the lattice parameters are estimated to be (+1%) and (−3%) along $\langle 1\,2\,3 \rangle_\delta$ and $\langle 1\,1\,1 \rangle_\delta$, respectively.

The electron diffraction pattern recorded along the zone axis $[\bar{5}\,4\,1\,0]_R \equiv [\bar{2}\,1\,0]_R /\!/ [0\,1\,\underline{1}]_\delta$ (Fig. 8) points out that the reflections $(0\,0\,0\,\overline{24})_{\boldsymbol{R}} \equiv (8 \times (0\,0\,0\,\bar{3})_{\boldsymbol{R}})$ and $(\bar{2}\,\bar{2}\,\bar{2})_\delta$ are not exactly overlapped. The measured misfit corresponds to a distance higher than $\frac{1}{6}a_\delta[1\,1\,1] = 0.082$ nm. This suggests that 23 equally spaced atomic layers parallel to $(1\,1\,1)_\delta$ will best describe the super unit cell. Upon that consideration, the atomic number becomes equal to $23 \times 7 = 161$ atoms. This compares favourably with the 159 atoms, which belong to the R-phase unit cell. The superimposition of the R-phase and the ferritic supercell structures along $[1\,1\,1]_\delta /\!/ [0\,0\,0\,1]_R$, points out that the atom displacements required to pass from the ferrite to the R-phase are less than interatomic distances. The departure to the

coherency between the R-phase and the ferritic matrix may be completely accommodated without any long-range strain fields by the introduction of dislocations. This analysis confirms that dislocations are potent sites for the R-phase nucleation.

3.5. Planar defects in the R-phase

Fine striations are observed on TEM images (Fig. 3) and streaks on diffraction parterns (Fig. 6). Streaks can arise from modifications of the shape of reciprocal lattice nodes either due to the shape of crystal defects or to the lattice strains associated with them [33]. These features reveal that the R-phase encountered in our specimens is heavily faulted. The streaking extent is indicative of extremely thin faults. As far as we are aware, faulted R-phases have never been reported for binary and ternary systems constituted with transition metals (Fe, Cr, Ni, Mo, W...) as reported in the literature [21–30]. In the present case, the high density of defects makes their identification very difficult with usual two-beam bright and dark field experiments. High-resolution (HREM) images (Fig. 9) issued of detailed investigation in progress indicate that the defects are similar to those encountered in the cubic Al_5Li_3Cu-phase which precipitates in Al-Li-Cu system [34].

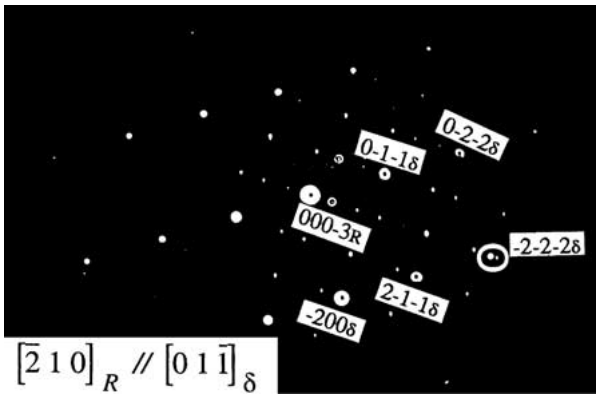

Figure 8 Electron diffraction pattern recorded along the $[\bar{5}\,4\,1\,0]_R \equiv [\bar{2}\,1\,0]_R /\!/ [0\,1\,1]_\delta$ zone axis pointing out that the reflections $(0\,0\,0\,\overline{24})_{\boldsymbol{R}} \equiv (8 \times (0\,0\,0\,\bar{3})_{\boldsymbol{R}})$ and $(\bar{2}\,\bar{2}\,\bar{2})_\delta$ are not exactly overlapped.

In order to determine the fault plane orientations, a schematic representation (Fig. 7) of the reciprocal lattice is rebuilt using the 3-D information given by the diffraction pattern taken along $[1\,1\,1]_\delta /\!/ [0\,0\,0\,1]_R$ (Fig. 10a). In that 3-fold axis diffraction pattern (Fig. 10a), the diffuse streaks form a honeycomb network between the Laue zones. Since the R-phase is described with a triple obverse hexagonal lattice; the structure factor is non-vanishing for all reflections with $(-h+k+1) \neq 3n$, where n is any integer. Hence, diffraction spots are only located in the Laue zones corresponding to the reciprocal layers 0, 3 and 6. The diffuse streaks, which are present between the Laue zones, are due to the intersection of the Ewald sphere with the tilted lines joining reciprocal nodes located in adjacent layers. Taking into account the 3-fold symmetry of the pattern, these lines are easily drawn in the reciprocal space using the hexagonal axis system (Fig. 7). They are the following directions: $[101]^*_R$, $[0\,\bar{1}\,1]^*_R$, $[\bar{1}\,1\,1]^*_R$, $[1\,0\,1]^*_R$, $[0\,1\,1]^*_R$ and $[1\,1\,1]^*_R$. The corresponding planes in the direct lattice are the fault planes.

Since we know the orientation relationships between the precipitates and the matrix, it is easy to determine the normals to the faulted planes in the hexagonal axes, using three digit-indices for convenience, and to tranfer them in the cubic system as indicated in Table III.

Conclusively, from this table, the fault planes can be grouped into sets parallel to $\{1\,3\,9\}_\delta$ and $\{11\,13\,23\}_\delta$. Without going into much detail, we should notice that the domains delimited by the families of defects $\{1\,3\,9\}_\delta$ and $\{11\,13\,23\}_\delta$ are represented by two types of polyhedron. This defects organization should be connected

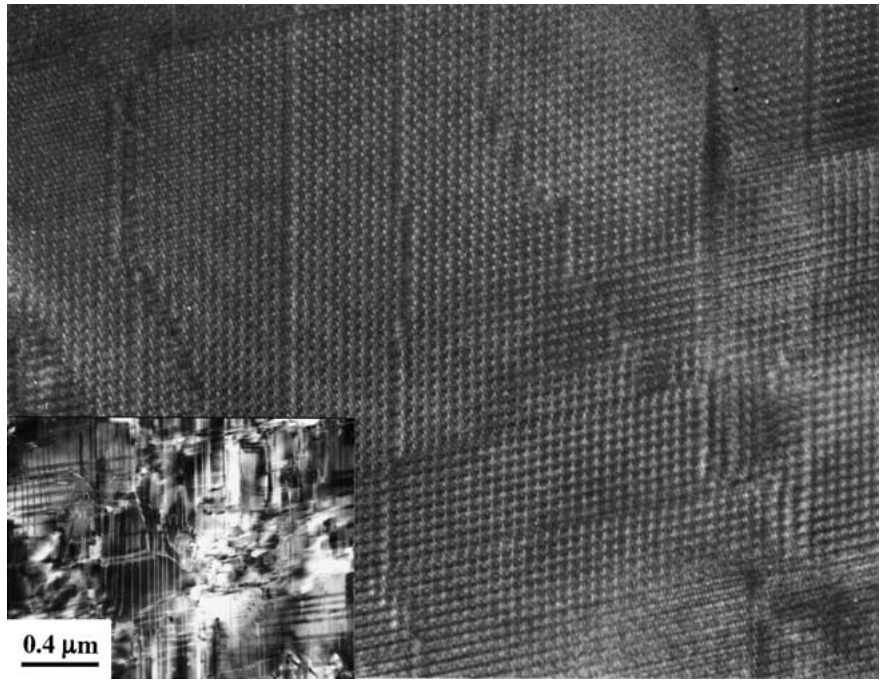

Figure 9 HREM image showing planar defects in R-phase particle. The inserted bright field TEM image points out the high density of defects.

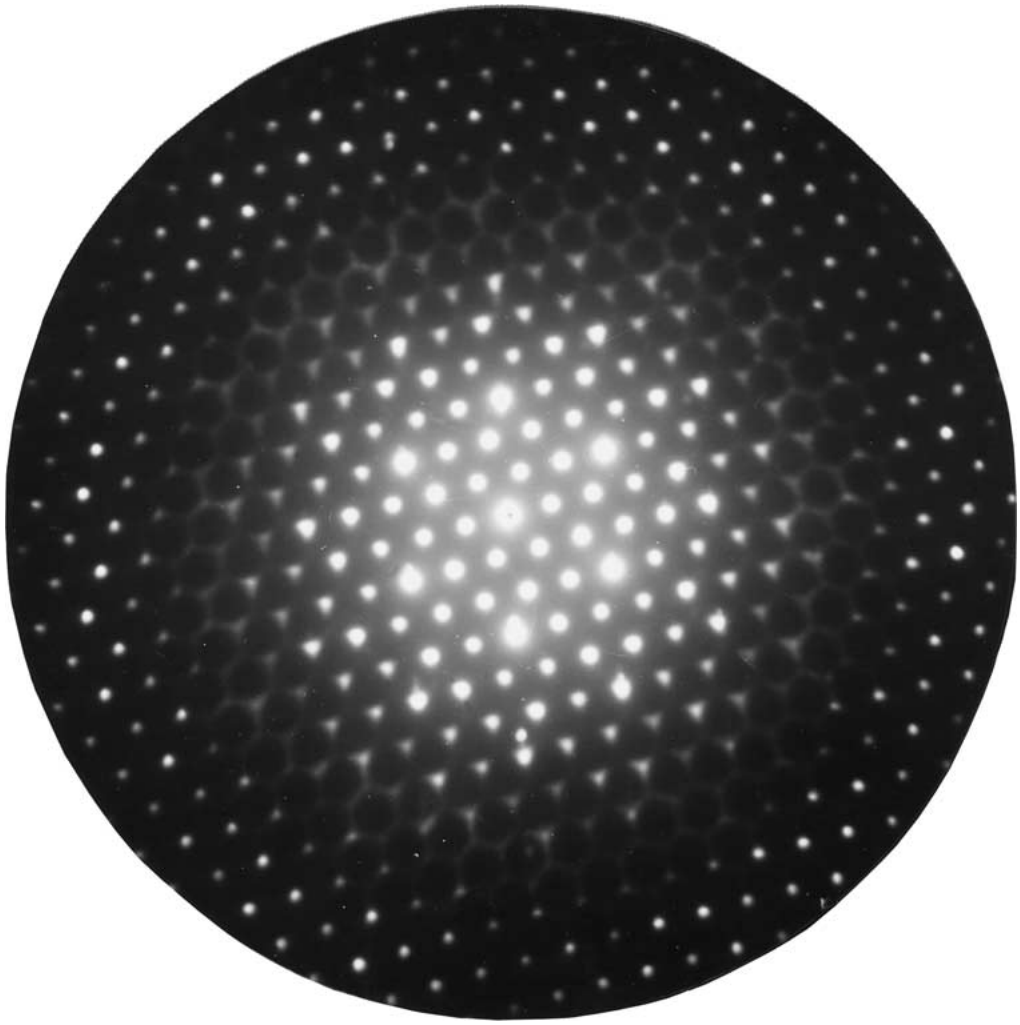

(a)

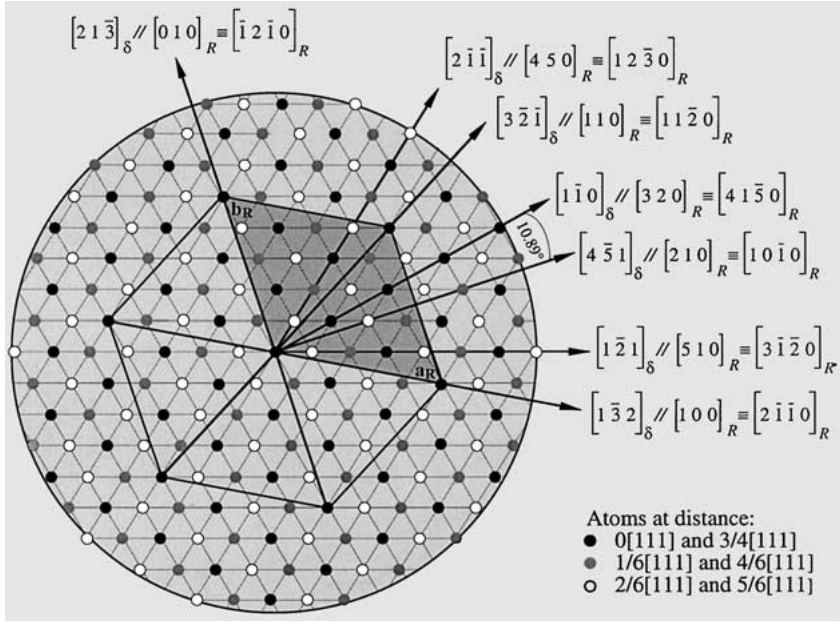

(b)

Figure 10 (a) Microdiffraction patterns recorded along the $[0\,0\,0\,1]_R$ zone axis showing the zeroth and the third order Laue zones. Since the lattice is described by means of a triple obverse hexagonal unit cell, the Laue zone which appears on the diffraction pattern is not the first-order Laue zone but the third one (TOLZ). Between the ZOLZ and the TOLZ, a honeycomb network is formed by the intersection of the Ewald sphere with the streaking lines due to the planar defects. (b) Projection of the atoms of the ferritic matrix onto the $(1\,1\,1)_\delta$ lattice plane. The dark grey lozenge corresponds to the ferritic supercell describing the R-phase.

TABLE III Defects planes in the R-phases are grouped in two families parallel respectively to $\{1\ 3\ 9\}_\delta$ and $\{11\ 13\ 23\}_\delta$ planes of the ferritic δ-matrix

Hexagonal axis system basis (Three and four-digit indices)	Matrix cubic system
$(1\,0\,1)_R = (1\,0\,\bar{1}\,1)_R$	$(23\ \overline{13}\ 11)_\delta$
$(0\,\bar{1}\,1)_R = (0\,\bar{1}\,1\,1)_R$	$(\overline{13}\ 11\ 23)_\delta$
$(\bar{1}\,1\,1)_R = (\bar{1}\,1\,0\,1)_R$	$(11\ 23\ \overline{13})_\delta$
$(1\,\bar{1}\,1)_R = (1\,\bar{1}\,0\,1)_R$	$(1\ \bar{3}\ 9)_\delta$
$(\bar{1}\,0\,1)_R = (\bar{1}\,0\,1\,1)_R$	$(\bar{3}\ 9\ 1)_\delta$
$(0\,1\,1)_R = (0\,1\,\bar{1}\,1)_R$	$(9\ 1\ \bar{3})_\delta$

to the fact that the R-phase is described by a stacking of polyhedra.

These defects planes have to be examined by means of the Frank and Kasper model used to describe defects in the σ, P, χ and μ intermetallic phases [20] whose structures are closely related with the R-phase and then to derive the vectors faults. A detailed study concerned with the vectors faults identification is in progress; the results have to be published in a forthcoming paper [45].

3.6. Morphology analysis, the equilibrium shape of the R-phase

The R-phase lattice is oriented with respect to the surrounding δ-ferritic matrix according to the orientation relationship as deduced from the recorded electron diffraction patterns (Fig. 6). This orientation relationship, which consists in making reference planes parallel, may be specified by the following variants:

$$(0\,0\,0\,1)_R /\!/ (1\,1\,1)_\delta$$
$$[\bar{2}\,\bar{1}\,\bar{1}\,0]_R \equiv [1\,0\,0]_R /\!/ [1\,\bar{3}\,2]_\delta$$
$$[\bar{1}\,2\,\bar{1}\,0]_R \equiv [0\,1\,0]_R /\!/ [2\,1\,\bar{3}]_\delta$$

Three and four digit-indices are used to make the symmetry elements in a prominent position.

It is well known that the morphology of transformation products, taking place in a solid matrix by diffusion-controlled mechanism or diffusionless mechanism (martensitic transformation) is of great importance in materials science. Understanding of both the equilibrium shape and the habit plane adopted and developed between the transformation products and the parent phase has been widely investigated. In the martensitic transformation, the optimum shape prediction has been successfully observed. For diffusion-controlled mechanism, several models [36–38] have been proposed and the morphology prediction, in the centre of the present study, has been of limited success.

It is well established that during nucleation of a precipitate in a supersaturated matrix, the reduction in free enthalpy is balanced by two opposed energies: the interface energy and the strain energy. In order to overcome these counteracting effects, nucleation of precipitation products generally occurs at structural heterogeneities in the microstructure where large elastic distortions already exist. As a result, precipitation of these second phases preferably occur at dislocations, interfaces and, most rapidly, at grain boundaries. To make easy the precipitation, particles often optimise orientation relationship with the parent matrix to give special shapes, namely: platelets, needles or spheroids. The morphology of newly forming precipitates strongly depends on the crystallographic orientation of the parent matrix.

In seeking to understand the observed morphology of particles, reference may be made to studies developed by different authors and reported in the literature [39, 40]. Both the morphology and the variant number of the precipitate, which adopts orientation relationships with the matrix, can be understood in terms of the group theory [39, 40]. This approach, based on the shared symmetry elements of the two point groups of product and parent phases, is applied here to explain R-phase precipitation features.

First of all, let us consider G^δ and G^R to be the symmetry point groups of the ferritic matrix and the decomposition product, the R-phase, respectively. The intersection point group of $G^\delta = m\ \bar{3}\ m$ and $G^R = \bar{3}$ is represented by their common symmetry elements when the precipitate adopts an orientation relationship with the matrix [39, 40]. This intersection point group, labelled $H (H = G^\delta \cap G^R)$, is one of the 32 crystallographic point groups and a subgroup of the matrix and of the precipitate point groups. We assert, with Cahn and Kalonji [40], that it is an error to relate the morphology of the precipitate to the symmetry of the matrix or of the precipitate. They suggest that the precipitate crystal adopts a form consistent with the symmetry of the subgroup H. Another important concept of the crystallographic symmetry is the index of the subgrouping which provides the number of precipitate variants of a given orientation relationship. Defined as the index of H in G^δ, the number of variants is the ratio of the order of G^δ to the order of H. The order of each point group represents its symmetry element number [41]. This symmetry concept has been successfully applied to determine the number of variants and to characterize the morphology of precipitates in differnt alloy systems [42, 43].

According to the orientation relationship developed by the R-phase with the δ-matrix, belonging to $m\ \bar{3}\ m$ and $\bar{3}$, respectively, the results of the symmetry analysis are summarized in Table IV.

For this orientation relationship, the 3-fold axes and inversion centres, common to δ and the R-phase, survive to the intersection point group. It is therefore clear that the shared symmetry elements lead to the intersection point group H:

$$H = G^\delta \cap G^R = \frac{4}{m}\,\bar{3}\,\frac{2}{m} \cap \bar{3} = \bar{3} \qquad (1)$$

The resulting point group $H = \bar{3}$ is the trigonal point group, the order of which is 6. It dictates the shape

TABLE IV Determination of the intersection point group H, the symmetry elements of which are common to the R-phase and the δ-ferritic matrix

Orientation relationship	Superimposed symmetries	Shared symmetries
$(0\,0\,0\,1)_R /\!/ (1\,1\,1)_\delta$	$3 /\!/ 3$	3
$[2\,\bar{1}\,\bar{1}\,0]_R \equiv [1\,0\,0]_R /\!/ [1\,\bar{3}\,2]_\delta$	$1 /\!/ 1$	1
$[\bar{1}\,2\,\bar{1}\,0]_R \equiv [0\,1\,0]_R /\!/ [2\,1\,\bar{3}]_\delta$	$1 /\!/ 1$	1

of R-phase particles. For this point group, the general forms developed are rhombohedra and the special ones are pinacoids and hexagonal prisms [44]. The equilibrium shape, which is consistent with the one experimentally, observed, is a pinacoid $\{0\,0\,0\,1\}_\delta$, i.e., elongated along $\langle 1\,1\,1\rangle_\delta$ direction of the ferritic matrix (Fig. 3).

The orientation relationship leading to the point group $H = \bar{3}$ is not at a symmetry dictated extremum with respect to relative rotation about the common axis $[0\,0\,0\,1]_R /\!/ [1\,1\,1]_\delta$, i.e., the 3-fold axis. However, extrema exist with respect to rotation, which would splay the superimposed symmetry elements [37–38].

Defined as the index H in G^δ, the number of variants is the ratio of the order of G^δ to that of H, i.e. $\frac{48}{6} = 8$ [39, 40]. This means that for the R-phase, there are 8 variants that could take place in every grain of the matrix.

3.7. X-ray spectroscopy microanalysis

In an attempt to assess the composition of the R-phase, to establish the distribution of the alloying elements and to compare it to that of the ferritic matrix, microanalysis was performed using energy-dispersive X-ray spectroscopy (EDS). Analyses were carried out in the thinnest areas of the foil, very close to the electrochemical hole. For the quantitative analysis, the K edge of the various elements (Fe, Cr, Ni, Mo, Mn and Si) was used. The quantification of the EDS spectra used for the Fe, Cr, Mo and Mn peak shapes was acquired from standards for a least-squares fitting and k factor calculation. For the statistical analysis, all the spectra for which the χ^2 of the fit was <4 were kept and even in this case the deviation of calculated concentration was always less than 3–5%. This uncertainty can be considered as a normal error inherent to the method used for quantification. Under these circumstances, the obtained results show that the chemical composition of the R-phase is homogeneous from particle to particle. The different results of the chemical analysis, listed in Table I, do not coincide with that of the same phase reported in the literature [30]. They show that precipitation of the R-phase leads to an alteration of the surrounding ferritic matrix.

Compared with the chemical composition obtained from the adjacent δ-ferrite, the elemental partitioning of Cr, Mn, Ni and Si in the R-phase is nearly the same when compared to that in the δ-matrix. It has been also pointed out that the R-phase is richer in Mo than the matrix (18 times more than in the matrix). However, it is interesting to note that the sums of both concentrations (Fe + Mo) are nearly the same in the two phases, but Mo in the R-phase largely substitutes Fe. This feature seems to support conclusively the idea that Mo promotes the precipitation of the R-phase as it does for the other χ and τ intermetallic phases [13, 18]. The R-phase particles contain as much as 30% Mo, a concentration smaller than the level (40%) leading to the pitting corrosion [30].

It is interesting to outline the role of Mo in this duplex stainless steel. At the longer ageing times and at high temperatures of its formation domain, the R-phase is the dominant constituent exhibiting coarsening particles in the vicinity of the austenite. The latter phase develops with rejection of Cr and Mo, which are efficient forming elements of the intermetallic phases, in the ferritic matrix. Chromium and especially Mo promote the nucleation and the development of the R-phase.

From the derived orientation relationship, we have stated that the compact $[1\,1\,1]_\delta$ direction of the ferrite is set parallel to $[0\,0\,0\,1]_R$. Komura *et al.* [21] have established the following occupancy percentage of Mo in the polyhedra: CN16 (100%), CN14 and CN15 (60%), the stacking of which is parallel to $[0\,0\,0\,1]_R$. In the ferritic matrix, Mo should occupy the larger sites, i.e., the centre of the BCC unit cell and are favourably stacked along $[1\,1\,1]_\delta /\!/ [0\,0\,0\,1]_R$. This suggests that in the supersaturated and unstable ferrite, a supercell structure of the R-phase pre-exists. The analysis of the similarities between the distribution of the atoms in the R-phase and in the ferritic supercell now allows us to say that the alteration of the ferritic matrix during the formation of the other phases: α'-BCC ferrite, τ-phase and austenite, leads to an unstable ferrite. When the ferritic matrix reaches a critical chemical composition close to that of the R-phase, the latter precipitate under favourable conditions, i.e., a complete matching is achieved between the position of the metal atoms in the matrix and in the R-phase by atomic position readjustments whose amplitudes are smaller than the interatomic distances.

The incubation time recorded for the R-phase formation corresponds to the time needed to reach the critical chemical composition. This feature is consistent with the assumption that the incubation time, around 85 hours, is associated with the low diffusivity of the Mo atom in the ferrite, when compared to the other transition metals.

4. Conclusion

The isothermal heat treatment of a duplex ($\delta + \gamma$) stainless steel in the temperature range 550–650°C leads to a series of metallurgical transformations, which mainly take place in the ferritic matrix. This study has been focused on the R-phase, an intermetallic compound, which belongs to the family of Frank-Kasper phases.

The characterization by electron microdiffraction determines unambiguously that the R-phase crystallizes in the trigonal system and belongs to the $R\bar{3}$ space group. The results of this electron diffraction characterization are in agreement with those reported from X-ray and neutron diffraction experiments.

The R-phase appears in association with spearhead-like morphology austenite [14], α'-BCC ferrite [15] and τ-phase, a novel intermetallic compound, the structure of which has been published elsewhere [18]. The R-phase precipitates nucleate on dislocations and grow with a lenticular shape extended along $\langle 1\,1\,1\rangle_\delta$ direction. The morphology and the variant number of this R-phase are understood in terms of the group theory. The electron diffraction pattern analysis generates the following orientation: $(0\,0\,0\,1)_R /\!/ (1\,1\,1)_\delta$ with $[1\,\bar{3}\,2]_\delta /\!/ [2\,\bar{1}\,\bar{1}\,0]_R$. The fact that this orientation relationship is obeyed is related to the occurrence of a good matching of the two structures in the direction normal to the plane of reference as well as in the plane of reference itself.

TEM observations and microdiffraction analyses revealed that R-phase particles are heavily faulted. As far as we know, this has not been reported for R-phases studied previously [21–31]. The defects are identified as planar faults, which are grouped into two families parallel respectively to $\{1\ 3\ 9\}_\delta$ and $\{11\ 13\ 23\}_\delta$ lattice planes of the ferritic δ-matrix. This defects organization should be connected with the fact that the R-phase is described by a stacking of polyhedra.

The orientation relationship developed between the matrix and the R-phase strongly suggests that the latter can be considered as a supercell of the ferritic matrix, i.e., a supercell structure of the R-phase. This supercell can be described as a stacking of 23 equally spaced atomic layers parallel to $(1\ 1\ 1)_\delta$. The latter are parallel to $(0\ 0\ 0\ 1)_R$, the basal plane of the R-phase. Each layer contains 7 atoms leading to 161 atoms, favourably compared with the 159 atoms, belonging to the R-phase unit cell. With an atomic plane stacked in less in comparison with that of the matrix, the R-phase nucleates on dislocations in order to accommodate this negative misfit. The R-phase is an intermetallic phase rich in Mo the presence of which plays an important role in promoting its formation and development.

Acknowledgements

One of the authors (A.R) is grateful to Dr. P. Ruterana (Ecole Polytechnique de Lausanne, Switzerland; Present address: LERMAT, Caen, France) for the chemical analysis by EDS and for HREM observations.

References

1. R. M. DAVISON and J. M. REDMOND, *Mater. Performance* **29** (1990) 57.
2. H. KIESHEYER, in Proceedings of the International Conference on Stainless Steels' 91 (The Iron and Steel Institute of Japan, Chiba, Japan 1991) p. 1148.
3. V. J. DIGGS, W. D. BUSKO and C. M. SCHILLMOLLER, in Proceedings of the International Conference on Duplex Stainless Steels'91, edited by J. Charles and S. Bernhardsson (Les Editions de Physique, Les Ulis, 1991) Vol. 2, p. 1163.
4. D. J. A. FRUYTIER, in Proceedings of the International Conference on Duplex Stainless Steels'91, edited by J. Charles and S. Bernhardsson (Les Editions de Physique, Les Ulis, 1991) Vol. 2, p. 497.
5. I. TAMURA and Y. TOMOTA, in Proceedings of the Symposium on Mechanical Behaviour of Materials (Japan Society of Materials Science, Kyoto, 1974) Vol. 2, p. 105.
6. J. FOCT, N. AKDUT and G. GOTTSTEIN, *Scripta Metall. Mater.* **27** (1992) 1033.
7. N. SRIDHAR, J. KOLTS and L. H. FIASCHE, *J. Metals* **37** (1985) 31.
8. T. MAGNIN and J. M. LARDON, *Mater. Sci. Eng.* A **104** (1988) 21.
9. S. BERNHARDSSON, J. OREDSSON and C. MARTENSON, in Proceedings of the International Conference on Duplex Stainless Steels'82, edited by R. A. Lula (ASM, Metals Park, OH, 1983) p. 267.
10. J. C. PROUHEZE, J. C. VAILLANT, G. GUNTZ and B. LEFEBVRE, in Proceedings of the International Conference on Duplex Stainless Steels'82, edited by R. A. Lula (ASM, Metals Park, OH, 1983) p. 247.
11. H. D. SOLOMON, in Proceedings of the International Conference on Duplex Stainless Steels'82, edited by R. A. Lula (ASM, Metals Park, OH, 1983) p. 41.
12. J. CHARLES, in Proceedings of the International Conference on Duplex Stainless Steels'91, edited by J. Charles and S. Bernhardsson (Les Editions de Physique, Les Ulis, 1991) Vol. 2, p. 3.
13. A. REDJAÏMIA, Thèse de Doctorat d'Etat, Institut National Polytechnique de Lorraine, Nancy, France, 1991.
14. A. REDJAÏMIA and G. METAUER, *J. Mater. Sci.* **36** (2001) 1717.
15. A. REDJAÏMIA, G. METAUER and M. GANTOIS, *Scripta Metall. Mater.* **25** (1991) 1879.
16. R. LAGNEBORG, *Trans. Am. Soc. Metals* **60** (1967) 67.
17. A. MATEO, L. LLANES, M. ANGLADA, A. REDJAÏMIA and G. METAUER, *J. Mater. Sci.* **32** (1997) 4533.
18. A. REDJAÏMIA, P. RUTERANA, G. METAUER and M. GANTOIS, *Phil. Mag.* A **67**(5) (1993) 1277.
19. E. L. BROWN and G. GRAUSS, *Metall. Trans.* **14** (1983) 791.
20. F. C. FRANK and J. S. KASPER, *Acta Crystallogr.* **11** (1958) 184.
21. Y. KOMURA, W. G. SLY and D. P. SHOEMAKER, *ibid.* **13** (1960) 575.
22. C. B. SHOEMAKER, D. P. SHOEMAKER and J. MELLOR, *ibid.* **18** (1965) 37.
23. H. HUGUES, and S. R. KEOWN, *J. I. S. I.* **206** (1968) 275.
24. D. J. DYSON and S. R. KEOWN, *Acta Metall.* **17** (1969) 1095.
25. F. A. THOMPSON and D. R. F. WEST, *J. I. S. I.* **209** (1972) 691.
26. P. JOLLY and J. HOCHMANN, *Mémoires Scientifiques Rev. Métallurg.* **2** (1973) 117.
27. J. M. HAUDIN and F. MONTHEILLET, *Metallography* **11** (1978) 391.
28. S. KOBAYASHI, K. NAKAII and Y. OHMORI, *Acta Mater.* **49** (2001) 1891.
29. S. P. REDEOUT, W. D. MANLY, E. L. KAMEN, B. S. LEMENT and P. A. BECK, *Trans. Amer. Inst. Min. (Metall.) Engrs.* **191** (1951) 872.
30. J. O. NILSON and P. LIU, *Mater. Sci. Technol.* **7**(9) (1991) 853.
31. A. REDJAÏMIA and G. METAUER, to be published.
32. J. P. MORNIROLI and J. W. STEEDS, *Ultramicroscopy* **45** (1992) 219.
33. J. W. EDINGTON, "Practical Electron Microscopy in Materials Science," Vol. 3 (Philips Eindhoven, 1974) p. 67.
34. P. DONNADIEU, *Phil. Mag.* A **64** (1) (1991) 97.
35. T. HAHN (ed.) "International Tables for Crystallography" (Reidel, Dordrecht, 1988)
36. W. BOLLMANN, *Phys. Stat. Sol. (a)* **21** (1974) 543.
37. R. W. BALLUFI, A. BROKMANN, H. KING, *Acta Metall.* **30** (1982) 1453.
38. U. DAHMEN, *ibid.* **30** (1982) 63.
39. R. PORTIER, D. GRATIAS, *J. Phys. Sup.* **43**(12) (1982) C4.
40. J. W. CAHN and G. KALONJI, in Proceedings of the Conference on Solid-Solid phase Transformations, edited by H. I. Aaronson, R. F. Sekereka, D. E. Laughlin and C. M. Waymann (Metall. Soc. AIME, Warrendale, 1982) p. 3.
41. M. J. BUERGER, "Elementary Crystallography" (Massachussetts Institute of Technology Press, Cambridge, 1978).
42. B. C. MUDDLE and I. J. POLEMAR, *Acta Metall.* **36** (1989) 777.
43. A. BENLAMINE, R. PORTIER, J. P. SENATEUR and F. REYNAUD, *Scripta Metall.* **19** (1985) 63.
44. F. C. PHILLIPS, "An Introduction to Crystallography," 4th ed. (Longman, Singapore, 1971).
45. A. REDJAÏMIA, A. PROULT, J. P. MORNIROLI, P. DONNADIEU and G. METAUER, to be published.

Received 17 December 2001
and accepted 3 June 2002